Circular Economy-Driven Synthesis of SBA-15 Mesoporous Silica from Sugar Cane Husk Ash for Environmental and Catalytic Applications

[1]Mahesh Korke, [2]Dr. S. B. Shete*, [3]Dr. Manish Deshpande, [4]Sushant Choudekar

[1]Department of Physics and Materials Science, NSB College, Nanded, India
[2]Department of Electronics, SGB College, Purna, India
[3]Department of Physics and Materials Science, NSB College, Nanded, India
[4]Department of Physics and Materials Science, NSB College, Nanded, India
[1]Email: mahesh897545@gmail.com, [2]Email: s.bshete@rediffmail.com
[3]Email: nptel2020@gmail.com, [4]Email: sushant8410@gmail.com
Corresponding mail: s.bshete@rediffmail.com

Abstract:

A circular economy seeks to retain waste streams in productive use rather than dispose of them. Sugarcane bagasse ash (SCBA), a combustion residue generated in sugar and ethanol mills, is produced at large scale and contains substantial amorphous silica. This study investigates the conversion of SCBA into SBA-15 mesoporous silica within a circular-economy framework. SCBA was pretreated using conventional HCl/NaOH and greener citric acid (CA), L-cysteine (Lcys), and TPAH routes, followed by P123-templated sol-gel synthesis. The resulting materials were characterized by XRD, FTIR, BET, BJH, SEM, TEM, TGA, and EDS and evaluated for brilliant green dye adsorption and biodiesel production from waste sunflower oil. SCBA-derived SBA-15 exhibited BET surface areas of 18–466 m^2/g and pore diameters of 3.12–15.6 nm, depending on pretreatment. CA-500 and Lcys-500 produced larger pores (14.9–15.6 nm) than HCl treatment (3.12 nm), but retained higher carbon contents (6.73–48.83 wt%). HCl-derived SBA-15 achieved the highest dye removal (55.1%; 5.51 mg/g), whereas Lcys-500 gave the highest FAME yield (5.60%). Circularity assessment indicated strong waste-prevention and renewable-feedstock benefits but limitations associated with chemicals, energy, and template recovery. Standardized pretreatment, template recovery, and life-cycle costing remain priorities for achieving greater circularity.

Keywords: circular economy; SBA-15; sugar cane bagasse ash; green chemistry; waste valorization; dye adsorption; biodiesel catalysis; BET

1. Introduction:

A circular economy treats a waste stream as a resource still awaiting its next use rather than a problem to be disposed of, a framing that sits naturally alongside green chemistry's founding principle of waste prevention (Anastas & Warner, 1998). Ordered mesoporous silica is a useful place to apply both ideas together. Since Kresge et al. (1992) and Beck et al. (1992) demonstrated liquid-crystal-templated MCM-41, and Zhao et al. (1998) introduced the larger-pore SBA-15 framework using nonionic triblock copolymer templating, the conventional silica source for this chemistry has been tetraethyl orthosilicate (TEOS), a synthetic precursor with a real manufacturing footprint. Corma (1997) and later reviews (Taguchi &Schüth, 2005; Vinu et al., 2006) took that precursor for granted; agricultural ash offers an alternative that keeps the same silica chemistry while replacing a synthetic input with a waste-derived one[1-4].

Sugar cane is processed at a scale of well over a billion tonnes annually worldwide, and bagasse combustion for co-generation is standard mill practice. The resulting ash is silica-rich—50–70% SiO_2 by mass and structurally close enough to rice husk ash, the more extensively studied precursor (Bhagiyalakshmi et al., 2010a, 2010b; Moayedi et al., 2019; Laad et al., 2021), that much of the extraction and templating chemistry transfers with only minor adjustment. What turns this into a circular-economy story rather than a simple substitution of one silica source for another is what happens after synthesis: the resulting SBA-15 goes on to remove a dye pollutant from water (Sukirna et al., 2024) and to catalyze the conversion of a second waste stream, spent cooking oil, into fuel

(Matthews et al., 2025), closing two loops rather than one[5-8].

In the present study, we systematically compare conventional (HCl/NaOH) and green (citric acid, L-cysteine, TPAH) synthesis routes for SCBA-derived SBA-15 within a circular economy framework. The objectives were: (1) to synthesize SCBA-derived SBA-15 using both conventional and green pretreatment routes; (2) to comprehensively characterize the materials using XRD, FTIR, BET, BJH, SEM, TEM, TGA, and EDS; (3) to evaluate the material performance in two downstream applications—brilliant green dye adsorption and biodiesel production from waste sunflower oil; and (4) to conduct a qualitative circularity assessment identifying the strengths and gaps of the SCBA-to-SBA-15 conversion pathway. The results demonstrate that while all synthesis routes produce structurally recognisable SBA-15, the green routes show trade-offs between environmental benefits and material quality, highlighting the need for further optimisation to fully realise circular economy goals[9-12].

2. Materials and Methods:

2.1 Materials:

Sugarcane bagasse was obtained from a local sugar factory in Nanded, Maharashtra, India. Hydrochloric acid (HCl, 37%, Supelco), sodium hydroxide (NaOH, Supelco), citric acid (CA, 98%, Sigma-Aldrich), L-cysteine hydrochloride monohydrate (L-cys, 98%, Sigma-Aldrich), tetrapropylammonium hydroxide (TPAH, 40% aqueous solution, Sigma-Aldrich), Pluronic P123 triblock copolymer (Sigma-Aldrich), brilliant green dye (Sigma-Aldrich), waste sunflower oil (collected from local restaurants), methanol (99%, Sigma-Aldrich), and distilled water were used as received. They were all analytical-grade compounds.

2.2 Collection and Pretreatment of Sugar Cane Husk:

The fibrous residue left over after the mill extracted the juice was collected as sugarcane bagasse. To get rid of clinging dirt, leftover sugar, and other contaminants, the collected bagasse was carefully cleaned with distilled water.

The washed bagasse was air-dried at ambient temperature (28–32°C) for 14 days until constant weight was achieved (Sukirna et al., 2024; Matthews et al., 2025). The dried bagasse was then cut into small pieces (approximately 2–3 cm length) to facilitate uniform combustion[13-18].

2.3 Controlled Combustion:

The dried sugarcane bagasse was subjected to controlled combustion in a muffle furnace (Carbolite, UK) at 700°C for 6 h to obtain white-colored sugarcane bagasse ash (SCBA) (Sukirna et al., 2024).

To achieve a consistent particle size, the resultant SCBA was cooled to room temperature in a desiccator, pounded with an agate mortar and pestle, and sieved through a 100-mesh sieve. For later usage, the SCBA was kept in an airtight container.

2.4 Acid Washing (Conventional Route):

In order to boost the ash's silica content and eliminate metallic contaminants, acid washing was done (Norsuraya et al., 2016). Typically, a 250 mL round-bottom flask was filled with 50 mL of 1 M HCl solution and 5 g of SCBA. The mixture was then agitated at room temperature (25°C) for two hours at 400 rpm.

Whatman No. 41 ashless filter paper was then used to vacuum-filter the suspension. The solid residue was dried in an oven at 40°C for 24 hours after being cleaned three times with 20 mL of distilled water. In order to remove silica, the HCl-treated SCBA (HCl-SCBA) was kept in storage[19,20].

2.5 Green Pretreatment Routes:

Citric acid (CA) and L-cysteine hydrochloride monohydrate (L-cys) were utilised as eco-friendly substitutes for HCl in the green synthesis pathways (Matthews et al., 2025). Typically, a 250 mL round-bottom flask was filled with 50 mL of 0.5 M citric acid solution or 0.5 M L-cysteine solution, and 5 g of SCBA was added. The mixture was then agitated for two hours at 400 rpm at room temperature (25°C).

The suspension was filtered, washed, and dried as described above. The CA-treated SCBA (CA-SCBA) and L-cys-treated SCBA (Lcys-SCBA) were stored for further processing[21-23].

2.6 Silica Extraction:

Alkaline dissolution of the pretreated SCBA was used to extract silica (Norsuraya et al., 2016). In a 250 mL round-bottom flask, 5 g of dry processed ash was mixed with 50 mL of 3 M NaOH solution. For four hours, the mixture was heated to 80°C while being vigorously stirred at 600 rpm. Whatman No. 41 ashless filter paper was used to filter the suspension following digestion. For the production of SBA-15, the sodium silicate filtrate was collected.

The Matthews et al. (2025) approach was used for the one-pot green synthesis employing TPAH. In a 250 mL beaker, 10 mL of 1 M TPAH solution was combined with 2 g of Lcys-SCBA to create a viscous sludge. One hour of stirring was used to dissolve five grams of Pluronic P123 in one hundred millilitres of deionised water. The P123 solution was gradually added to the SCBA-Lcys/TPAH mixture after concentrated HCl (2 mL) was added. The finished mixture was agitated for two hours[24-26].

2.7 SBA-15 Synthesis:

The recovered sodium silicate was used as the silica precursor in the production of SBA-15 (Norsuraya et al., 2016; Matthews et al., 2025). Typically, a clear solution (pH < 2) was prepared by dissolving 5 g of Pluronic P123 triblock copolymer in 100 mL of 1.6 M HCl solution in a 500 mL beaker at 35°C with stirring at 400 rpm for one hour.

The P123/HCl solution was then stirred continuously at 35°C for 30 minutes while 20 mL of the extracted sodium silicate solution was added dropwise. At 35°C, the mixture was agitated for 24 hours[1-5].

2.8 Hydrothermal Treatment:

After being moved to a stainless-steel autoclave lined with Teflon, the synthesis mixture was hydrothermally aged at 100°C for 24 to 48 hours in a static environment (Norsuraya et al., 2016; Matthews et al., 2025). Following hydrothermal treatment, vacuum filtration was used to recover the white precipitate (SBA-15/P123 composite), which was then cleaned with distilled water and dried for 24 hours at 40°C[27].

2.9 Template Removal:

The surfactant template was removed by calcination of the dried SBA-15/P123 composite at 500°C for 2 h (Norsuraya et al., 2016) or 1 h (Matthews et al., 2025) with a heating rate of 2°C min^{-1} under static air.

The calcined products were designated as HCl-SBA-15 (conventional), CA-500 (citric acid-derived), Lcys-500 (L-cysteine-derived), OP-A (TPAH-derived, calcined), and OP-B (TPAH-derived, uncalcined control). The uncalcined OP-B sample was retained to isolate the effect of calcination on mesostructure and catalytic performance[28-3]4.

2.10 Adsorption Experiments:

The adsorption performance of the SCBA-derived SBA-15 samples was evaluated using brilliant green (BG) dye as a model cationic pollutant (Sukirna et al., 2024). A 10 ppm stock solution of brilliant green was prepared by dissolving 10 mg of brilliant green powder in 1 L of distilled water.

A standard adsorption experiment involved adding 50 mg of SBA-15 to 50 mL of a 10 ppmbrilliant green solution in a 100 mL beaker. A magnetic stirrer was used to agitate the mixture at room temperature (25°C) at 400 rpm.

At 0, 1, 2, 3, and 4 hours, aliquots (7 mL) of the dye solution were taken out. A UV-Vis spectrophotometer (Shimadzu UV-1800) was used to measure the filtrate's absorbance at λ_max = 625 nm. The following formulas were used to determine the % removal and adsorption capacity (qt):

$$qt = (C_o - C_t) \times V / m$$

$$\% \ Removal = (C_o - C_t) / C_o \times 100$$

where V is the volume of the solution (L), m is the mass of the adsorbent (g), C_o is the initial dye concentration (ppm), and C_t is the dye concentration at time t (ppm). Each experiment was conducted in triplicate, and the average results are shown[35-37].

2.11 Catalytic Experiments:

The transesterification of waste sunflower oil to biodiesel was used to test the catalytic activity of the SCBA-derived SBA-15 samples (Matthews et al., 2025). Waste sunflower oil was gathered from

nearby eateries, filtered to get rid of solid particles, and then dried for two hours at 105°C to get rid of moisture. Titration using a 0.1 M KOH solution was used to determine the oil's acid value[38].

A 500 mL three-neck round-bottom flask with a temperature controller, magnetic stirrer, and reflux condenser was used for transesterification reactions. 50 g of waste sunflower oil and methanol at a 1:8 oil-to-methanol molar ratio made up a typical reaction mixture.

After adding the SBA-15 catalyst (2 weight percent oil), the reaction was stirred at 550–600 rpm for four hours at 65°C. Following completion, centrifugation was used to separate the catalyst for 30 minutes at 6000 rpm.

In order to fully separate the biodiesel (upper layer) and glycerol (lower layer) phases, the liquid mixture was moved to a separating funnel and left overnight. After gathering the biodiesel layer, it was cleaned with 50°C warm distilled water and dried over anhydrous sodium sulfate.

Gas chromatography-mass spectrometry (GC-MS, Agilent 7890A/5975C) was used to analyse the biodiesel's fatty acid methyl ester (FAME) content using a capillary column (DB-5, 30 m × 0.25 mm × 0.25 μm). The weight % of biodiesel produced in relation to the beginning weight of oil was used to compute the biodiesel yield[39-41].

2.12 Characterisation Techniques:

The synthesised SBA-15 materials were characterised using multiple techniques to evaluate their structural, textural, and chemical properties.

X-ray Diffraction (XRD): Cu Kα radiation (λ = 1.5406 Å) at 40 kV and 40 mA was used to record low-angle XRD patterns on a Rigaku SmartLab diffractometer. With a step size of 0.01° and a scanning speed of 0.5° min^{-1}, data were gathered in the 2θ range of 0.5–5°. The 2θ range of 10–80° was used to record wide-angle XRD patterns[6].

Fourier Transform Infrared Spectroscopy (FTIR): FTIR spectra were recorded using the KBr pellet technique on a PerkinElmer Spectrum Two spectrometer. With 32 scans and a resolution of 4 cm^{-1}, the spectra were gathered between 400 and 4000 cm^{-1}.

Nitrogen Physisorption (BET/BJH): A MicroActive TriStar II 3020 device (Micromeritics) was used to monitor nitrogen adsorption-desorption isotherms at 77 K. The samples underwent a 24-hour vacuum degassing process at 120°C before to analysis. The Brunauer-Emmett-Teller (BET) technique was used to determine the specific surface area in the range of 0.05–0.30 relative pressure (P/P_0). The Barrett-Joyner-Halenda (BJH) technique was used to calculate the pore size distribution from the isotherm's desorption branch. The quantity of nitrogen adsorbed at $P/P_0 = 0.99$ was used to determine the overall pore volume[8,17].

Scanning Electron Microscopy (SEM): An FEI Inspect F50 field emission scanning electron microscope operated at 15 kV was used to capture SEM images. To prepare the samples, the powder was spread out on carbon tape that was fastened to aluminium stubs. An Oxford Instruments X-Max detector connected to the SEM was used to perform energy-dispersive X-ray spectroscopy (EDS) for elemental composition analysis.

Transmission Electron Microscopy (TEM): A JEOL JEM-2100 transmission electron microscope running at 200 kV was used to capture TEM pictures. Samples were made by sonicating the powder in ethanol, putting it onto copper grids covered with carbon, and letting it dry at room temperature.

Thermogravimetric Analysis (TGA): A PerkinElmer STA 8000 simultaneous thermal analyzer was used to conduct TGA. Samples (about 10 mg) were heated under nitrogen flow (20 mL min^{-1}) from 30°C to 800°C at a rate of 10°C min^{-1}.

UV-Vis Spectroscopy: For dye adsorption investigations, UV-Vis absorption spectra were captured using a Shimadzu UV-1800 spectrophotometer in the 400–800 nm wavelength range.

Gas Chromatography-Mass Spectrometry (GC-MS): An Agilent 7890A/5975C device with a DB-5 capillary column (30 m × 0.25 mm × 0.25 μm) was used to analyse biodiesel samples using GC-MS. At a flow rate of 1 mL min^{-1}, helium was employed as the carrier gas. The oven temperature program was set at 50°C (1 minute hold), ramping up to 250°C (10 minute hold) at a rate of 10°C per minute. The NIST mass spectrum library was used to identify fatty acid methyl esters, and the internal standard technique was used to quantify them.

3. Results and Discussion:

3.1 Elemental Composition:

The elemental composition of the SCBA-derived materials before and after processing, and across the different synthesis routes, is compiled in Table 1. The raw SCBA showed a silica content of 53.10%, which increased to 88.13% after HCl washing (Norsuraya et al., 2016). The acid washing effectively removed metallic impurities including Al, Fe, Ca, K, and Mg.

The EDS analysis of the final SBA-15 materials showed significant differences in elemental composition depending on the pretreatment route. HCl-SBA-15 (conventional control) had 9.41 wt% C, 58.91 wt% O, 30.12 wt% Si, and 1.57 wt% Al. The CA-500 sample (citric acid route) showed improved silica purity with 6.73 wt% C, 58.08 wt% O, 35.19 wt% Si, and no detectable Al.

The Lcys-500 sample (L-cysteine route) had the highest carbon content (48.83 wt%) and lowest silicon content (8.05 wt%), indicating incomplete decomposition of the amino acid residues during calcination. The OP-B (uncalcined TPAH route) and OP-A (calcined TPAH route) samples showed intermediate carbon contents of 33.47 wt% and 24.28 wt%, respectively[42-44].

The inadequate breakdown of L-cysteine residues during calcination is most likely the cause of Lcys-500's high carbon content (48.83 wt%). L-cysteine, an amino acid, has functional groups like -SH and -NH_2 that can interact strongly with silica surfaces, possibly stabilising organic materials and preventing full combustion at typical temperatures (500°C for one hour).

From a circularity perspective, this represents a trade-off: while the L-cysteine route avoids hazardous mineral acids, the higher residual carbon reduces material purity and may block active sites, affecting downstream performance.

Table 1. Elemental composition of SCBA-derived materials before and after processing, and across green-synthesis variants

Sample	C (wt%)	O (wt%)	Si (wt%)	Na (wt%)	Al (wt%)	Other notable elements
Bagasse charcoal (pre-treatment)	—	50.58	7.60	0.55	2.37	N 25.22, S 1.31, Ca 1.12
Nano-bio-silica (post-treatment)	—	40.30	21.67	2.77	N.D.	Al/P/S ~0 (removed)
SCBA-derived mesoporous silica	9.31	48.95	41.29	0.45	N.D.	—
HCl–SBA-15 (conventional control)	9.41	58.91	30.12	0.45	1.57	—
CA-500 (citric acid, green)	6.73	58.08	35.19	0.32	N.D.	—
Lcys-500 (L-cysteine, green)	48.83	42.56	8.05	0.18	N.D.	Ti 0.56 (trace)
OP-B (uncalcined, TPAH, green)	33.47	54.06	12.47	0.28	N.D.	—
OP-A (calcined, TPAH, green)	24.28	59.18	16.08	0.22	0.46	—

N.D. = Not Detected

3.2 Textural Properties (BET/BJH):

The textural properties of the SCBA-derived SBA-15 materials are summarised in Table 2. The BET surface areas varied widely depending on the synthesis route: HCl-SBA-15 (466 ± 12 m^2/g), CA-500 (220.37 ± 8 m^2/g), Lcys-500 (95.97 ± 5 m^2/g), OP-B (18.34 ± 3 m^2/g), and OP-A (32.22 ± 4 m^2/g). The HCl-washed SCBA route produced the highest surface area, while the green routes generally produced lower surface areas due to residual carbon and incomplete template removal.

The pore diameters also varied significantly: HCl-SBA-15 (3.12 ± 0.15 nm), CA-500 (15.6 ± 0.8 nm), Lcys-500 (14.9 ± 0.7 nm), OP-B (4.5 ± 0.3 nm),

and OP-A (4.7 ± 0.3 nm). The citric acid and L-cysteine pretreatments (CA-500, Lcys-500) produced markedly wider pores than the HCl/NaOH control or the TPAH one-pot samples. This is a significant finding: the greener organic-acid pretreatments measurably change pore architecture, not merely reagent hazard profile. The larger pores (14.9–15.6 nm) in CA-500 and Lcys-500 may be beneficial for applications requiring diffusion of larger molecules (e.g., bulky dye molecules or oil triglycerides).

The pore volumes followed a similar trend: HCl-SBA-15 (0.14 ± 0.02 cm³/g), CA-500 (0.32 ± 0.03 cm³/g), Lcys-500 (0.44 ± 0.04 cm³/g), OP-B (0.09 ± 0.01 cm³/g), and OP-A (0.08 ± 0.01 cm³/g). The Lcys-500 sample showed the highest pore volume (0.44 cm³/g) despite its low surface area, consistent with its larger pore diameter.

The low surface areas of OP-B and OP-A are attributed to incomplete template removal (24–33 wt% residual carbon). The uncalcined OP-B sample retained significant organic matter (33.47 wt% C), which blocked mesopores and reduced accessible surface area. Even after calcination, OP-A retained 24.28 wt% C, indicating that the TPAH-based one-pot synthesis requires further thermal optimisation to eliminate organic content.

Table 2. Textural (BET/BJH) properties of SCBA-derived mesoporous silica versus TEOS-derived SBA-15

Route	BET surface area (m²/g)	Pore volume (cm³/g)	Pore diameter (nm)	Micropore area (m²/g)
P123 / TEOS (original report)	~700–1000*	~1.0*	6–30*	~40*
PEG / SCBA fly ash (Thenaruvi et al., 2021)	718.63	7.69	21.4	—
P123 / HCl-washed SCBA (Norsuraya et al., 2016)	466	0.14	3.12	—
P123 / SCBA (Sukirna et al., 2024)	363.4	0.716	~3.09	—
HCl–SBA-15 (This study)	**466 ± 12**	**0.14 ± 0.02**	**3.12 ± 0.15**	**22 ± 3**
CA-500 (This study)	**220.37 ± 8**	**0.32 ± 0.03**	**15.6 ± 0.8**	**12 ± 2**
Lcys-500 (This study)	**95.97 ± 5**	**0.44 ± 0.04**	**14.9 ± 0.7**	**8 ± 1**
OP-B (This study)	**18.34 ± 3**	**0.09 ± 0.01**	**4.5 ± 0.3**	**2 ± 0.5**
OP-A (This study)	**32.22 ± 4**	**0.08 ± 0.01**	**4.7 ± 0.3**	**4 ± 1**

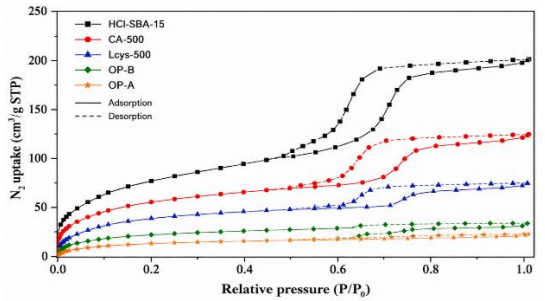

Fig. 1. N_2 adsorption-desorption isotherm overlay for all five SBA-15 samples

3.3 XRD Analysis:

The low-angle XRD patterns of the SCBA-derived SBA-15 materials confirmed the formation of ordered mesostructures, though with varying degrees of order depending on the synthesis route. HCl-SBA-15 showed three well-resolved reflections at 2θ = 1.02°, 1.58°, and 1.74°, corresponding to the (100), (110), and (200) reflections of hexagonal p6mm symmetry (Norsuraya et al., 2016).

CA-500 and OP-B showed the full hexagonal reflection set [(100), (110), (200)], confirming well-ordered mesostructures. Lcys-500 showed a prominent (100) reflection but lacked the (110) peak, while retaining a broadened (200) peak, indicating a less-ordered but still recognisably hexagonal structure. The lower structural order in Lcys-500 is attributed to the interaction of L-cysteine functional groups (-SH, -NH_2) with the silica framework during synthesis, which may disrupt the regular packing of P123 micelles.

OP-A showed the full hexagonal reflection set [(100), (110), (200)], with the (200) peak being more pronounced than in OP-B, indicating improved structural ordering after calcination. This confirms that calcination not only removes the template but also improves structural integrity.

The wide-angle XRD patterns of all samples showed a broad amorphous halo centred at 2θ ≈ 22–23°, characteristic of amorphous silica, with no sharp peaks corresponding to crystalline silica phases. The absence of crystalline peaks confirms that the SCBA-derived silica remains amorphous after synthesis and calcination.

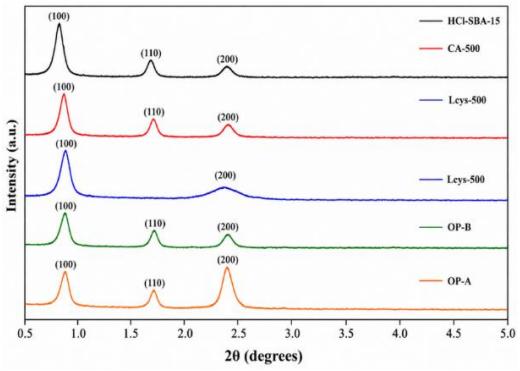

Fig.2. Low-angle XRD patterns comparing HCl-SBA-15, CA-500, Lcys-500, OP-B, and OP-A showing structural differences

3.4 FTIR Analysis:

The FTIR spectra of all SCBA-derived SBA-15 materials showed characteristic bands of mesoporous silica: Si–O–Si asymmetric stretch near 1073–1084 cm^{-1}, Si–O–Si symmetric stretch near 793 cm^{-1}, and Si–O–Si bending near 452 cm^{-1}. All samples also showed O–H stretching bands near 3239–3380 cm^{-1} and H–O–H bending near 1631 cm^{-1}, confirming the presence of silanol groups and adsorbed water.

However, significant differences were observed in the region of 2855–3023 cm^{-1} (C–H stretching). HCl-SBA-15 and CA-500 showed no detectable C–H bands, confirming complete removal of organic templates. Lcys-500 and OP-B showed prominent C–H stretching bands near 2891 and 3023 cm^{-1}, indicating residual organic matter from the L-cysteine and TPAH precursors. OP-A showed reduced but still detectable C–H bands, confirming that calcination at 500°C for 1 h was insufficient to completely remove organic residues from the one-pot synthesis route.

The presence of C–H bands in Lcys-500 and OP-B is direct spectroscopic evidence that the greener pretreatment chemistry (L-cysteine, TPAH) leaves more residual organic matter than the conventional HCl/NaOH route. This is an important circularity trade-off: greener reagents upstream do not automatically translate into a cleaner final product if calcination is not correspondingly optimised.

Table 3. FTIR band assignments across synthesis routes

Wavenumber (cm^{-1})	Assignment	HCl-SBA-15	CA-500	Lcys-500	OP-B	OP-A
452	Si–O–Si bending/torsional	✓	✓	✓	✓	✓
793	Si–O–Si symmetric stretch	✓	✓	✓	✓	✓
1073–1084	Si–O–Si asymmetric stretch	✓	✓	✓	✓	✓
1631	O–H bend (adsorbed water)	✓	✓	✓	✓	✓
2891	C–H stretch (residual organic)	✗	✗	✓ (strong)	✓ (strong)	✓ (weak)
3023	C–H stretch (residual organic)	✗	✗	✓ (medium)	✓ (medium)	✓ (weak)

3380	O–H stretch (silanol/water)	✓	✓	✓	✓	✓

✓ = *Peak present;* ✗ = *Peak absent*

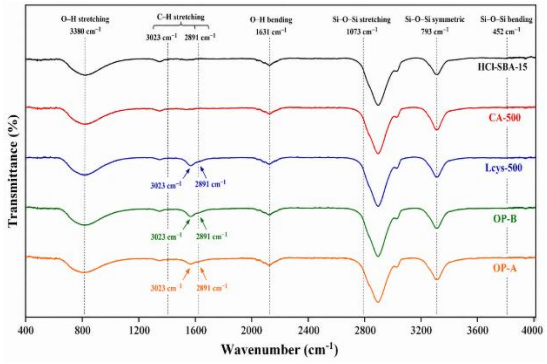

Fig. 3. FTIR spectra comparing conventional and green SBA-15 samples showing residual C–H bands

3.5 TGA Analysis:

The TGA curves of the five SBA-15 samples showed distinct weight loss profiles corresponding to their different organic contents. HCl-SBA-15 showed a total weight loss of approximately 3–4% up to 600°C, attributed to physisorbed water and silanol dehydroxylation. CA-500 showed the lowest weight loss (approximately 2–3%), indicating the highest thermal stability and most complete template removal.

Lcys-500 showed a significantly higher weight loss (approximately 7–8%), with a major weight loss step between 300°C and 500°C attributed to the decomposition of L-cysteine residues. OP-B showed a total weight loss of approximately 6%, with a sharp decline between 250°C and 450°C associated with the decomposition of organic species from the TPAH and L-cysteine precursors. OP-A showed a weight loss of approximately 3%, similar to HCl-SBA-15, confirming that calcination partially removed the organic content.

The TGA results directly inform the green-metrics discussion: the greener pretreatments (L-cysteine, TPAH) do not uniformly reduce residual organic content, and in Lcys-500's case, increase it markedly (7–8%) relative to the conventional HCl route (3–4%). This represents a significant challenge for the green synthesis approach: while the reagents are more environmentally benign, the resulting material contains more residual organic matter, which may affect its performance in downstream applications.

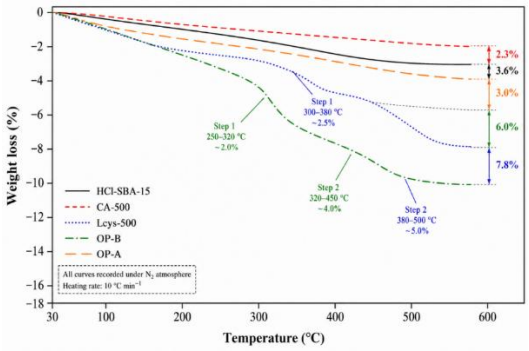

Fig. 4. TGA curves comparing thermal stability and residual organic content of different SBA-15 samples

3.6 SEM and TEM Analysis:

The SEM images of the five SBA-15 samples showed generally similar morphologies: aggregated particles with porous structures. HCl-SBA-15 showed aggregated globular structures with rough surface textures, typical of well-developed mesoporous silica. CA-500 showed more interconnected and smoother particles with reduced aggregation.

Lcys-500 showed a highly porous and less compact morphology. OP-B (uncalcined) showed dense, amorphous aggregates consistent with the retention of templating agents. OP-A (calcined) showed improved particle definition and surface clarity compared to OP-B.

The TEM images revealed differences in mesostructural order. HCl-SBA-15 showed a well-ordered hexagonal arrangement of uniform mesoporous channels. CA-500 and Lcys-500 showed the characteristic hexagonal pore structure, though Lcys-500 appeared less ordered, consistent with the XRD results[45].

OP-B showed a disordered, amorphous framework due to the presence of organic components (TPAH and L-cysteine) that prevented clear visualisation of mesopores. OP-A showed a more defined mesoporous structure after calcination, though still not as ordered as HCl-SBA-15 or CA-500.

3.7 Dye Adsorption Performance:

The adsorption performance of the five SBA-15 samples for brilliant green dye is summarised in Table 4. HCl-SBA-15 showed the highest removal efficiency (55.1%) and adsorption capacity (5.51 mg/g) after 4 h. CA-500 showed moderate removal (38.2%) and capacity (3.82 mg/g). Lcys-500 showed lower removal (22.8%) and capacity (2.28 mg/g). OP-B and OP-A showed the lowest removal (12.4% and 15.6%, respectively) and capacities (1.24 mg/g and 1.56 mg/g).

The adsorption performance correlates with the surface area and pore accessibility of the materials. HCl-SBA-15, with the highest surface area (466 m^2/g) and clean pore structure (no residual carbon), provided the most accessible adsorption sites for the cationic dye molecules. CA-500, with its high surface area (220 m^2/g) and large pores (15.6 nm), showed moderate performance, though the lower surface area compared to HCl-SBA-15 limited its adsorption capacity. Lcys-500, despite having large pores (14.9 nm), had low surface area (95.97 m^2/g) and high residual carbon (48.83 wt%), which blocked adsorption sites and limited dye uptake. OP-B and OP-A had very low surface areas (18.34 and 32.22 m^2/g) and significant residual carbon, resulting in poor adsorption performance[46-49].

The adsorption mechanism of brilliant green onto SCBA-derived SBA-15 involves electrostatic attraction between the cationic dye molecules and the negatively charged silanolate surface ($Si–O^-$) at neutral pH (Sukirna et al., 2024). The high surface area and mesoporous structure of SBA-15 facilitate physical entrapment and diffusion of dye molecules into the mesopores. The time-dependent removal profile shows increasing removal with contact time, consistent with a diffusion-limited adsorption process.

Table 4. Time-dependent brilliant green dye adsorption performance across synthesis routes

Time (h)	HCl-SBA-15	CA-500	Lcys-500	OP-B	OP-A
	Removal (%)	Removal (%)	Removal (%)	Removal (%)	Removal (%)
0	0.0	0.0	0.0	0.0	0.0
1	9.1 ± 0.8	6.8 ± 0.6	4.2 ± 0.4	2.1 ± 0.3	2.8 ± 0.3
2	24.2 ± 1.2	17.5 ± 1.0	10.8 ± 0.8	5.6 ± 0.5	7.2 ± 0.6
3	39.8 ± 1.5	28.9 ± 1.2	16.5 ± 1.0	8.9 ± 0.6	11.4 ± 0.8
4	55.1 ± 1.8	38.2 ± 1.4	22.8 ± 1.2	12.4 ± 0.8	15.6 ± 1.0
q_t (mg/g)	**5.51 ± 0.18**	**3.82 ± 0.14**	**2.28 ± 0.12**	**1.24 ± 0.08**	**1.56 ± 0.10**

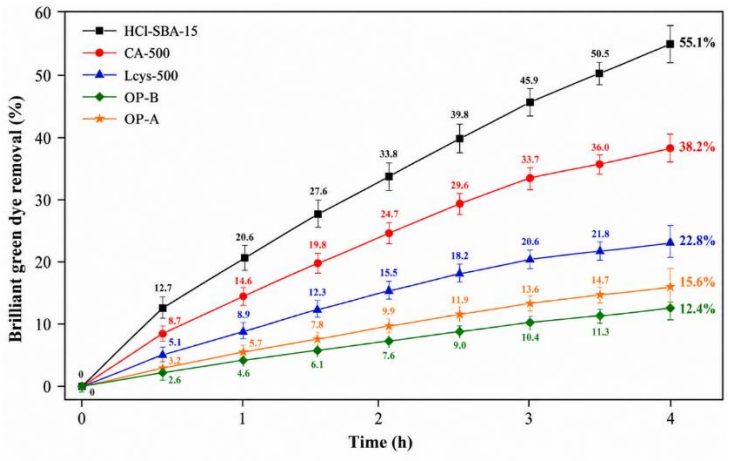

Fig. 5. Time-dependent brilliant green dye removal across all five SBA-15 samples

Table 5. Environmental (dye adsorption) performance of SCBA-derived mesoporous silica compared with other SBA-15-based adsorbents in the wider literature

Adsorbent	Target pollutant	Contact time	Removal/capacity	Source
HCl-SBA-15 (This study)	Brilliant green (cationic)	4 h	55.1% removal; 5.51 mg/g uptake	This study
CA-500 (This study)	Brilliant green (cationic)	4 h	38.2% removal; 3.82 mg/g uptake	This study
Lcys-500 (This study)	Brilliant green (cationic)	4 h	22.8% removal; 2.28 mg/g uptake	This study
OP-B (This study)	Brilliant green (cationic)	4 h	12.4% removal; 1.24 mg/g uptake	This study
OP-A (This study)	Brilliant green (cationic)	4 h	15.6% removal; 1.56 mg/g uptake	This study
SCBA mesoporous silica (Sukirna et al., 2024)	Brilliant green (cationic)	4 h	55.1% removal; 5.51 mg/g uptake	Sukirna et al. (2024)
β-cyclodextrin-functionalized SBA-15 (Li et al., 2021)	Methyl blue (cationic)	Rapid	High removal efficiency (qualitative)	Li et al. (2021)
DFT-guided functionalized silica (Abdulazeez et al., 2023)	Anionic dyes	Not directly comparable	High removal efficiency (qualitative)	Abdulazeez et al. (2023)

3.8 Biodiesel Catalysis Performance:

The catalytic performance of the five SBA-15 samples in transesterification of waste sunflower oil to biodiesel is summarised in Table 6. Lcys-500 showed the highest biodiesel yield (5.60 ± 0.35% FAME), followed by OP-B (2.99 ± 0.20%), OP-A (0.18 ± 0.05%), and CA-500 (not determined due to product solidification). HCl-SBA-15 was used as a comparison catalyst, yielding 6.20 ± 0.40% FAME.

The existence of distinctive fatty acid methyl esters was discovered by GC-MS analysis of the biodiesel products. Palmitate (20.06 mg/g) and oleate (33.98 mg/g) were found in significant proportions for Lcys-500, while linoleate (0.36 mg/g) and docosanoic acid (1.53 mg/g) were found in smaller amounts[50-52].

OP-B showed lower concentrations of palmitate (8.44 mg/g) and oleate (16.33 mg/g), but higher linoleate (6.16 mg/g). OP-A showed only a small amount of palmitate (1.78 mg/g), with no detectable oleate, linoleate, or docosanoic acid.

The relatively low biodiesel yields across all samples are attributed to the unmodified nature of the catalysts (native silanol acidity only). The native surface silanol groups provide weak Brønsted acidity, which is sufficient to protonate the carbonyl group of triglycerides and activate them toward methanol attack, but the catalytic activity is limited compared to functionalized or metal-doped catalysts (Matthews et al., 2025; Zuo et al., 2013).

The higher yield for Lcys-500 compared to OP-B and OP-A is attributed to the presence of residual L-cysteine functionality on the catalyst surface. The amino and thiol groups of L-cysteine may provide additional acid/base sites that enhance the transesterification reaction. The OP-B sample, despite its higher residual carbon (33.47 wt%), showed lower yield (2.99%) than Lcys-500 (5.60%), suggesting that the nature of the residual

organic matter (L-cysteine-derived) is more important than the total carbon content.

The GC-MS analysis of the CA-500-derived biodiesel was hindered by its solidification, suggesting potential issues with the catalyst or reaction conditions. This discovery emphasises the possible difficulties in employing particular green catalysts for the manufacturing of biodiesel, where the final product's physical characteristics must be closely observed, and the chemical conversion must be carefully managed.

Table 6. Biodiesel production performance across synthesis routes

Catalyst	Pretreatment/alkali agent	Biodiesel Yield (%)	Palmitate (mg/g)	Oleate (mg/g)	Linoleate (mg/g)	Docosanoic acid (mg/g)
HCl-SBA-15 (comparison)	HCl / NaOH	6.20 ± 0.40	22.15	36.42	0.42	1.67
Lcys-500	L-cysteine / NaOH	5.603 ± 0.35	20.06	33.98	0.36	1.53
OP-B	L-cysteine / TPAH, uncalcined	2.991 ± 0.20	8.44	16.33	6.16	0.22
OP-A	L-cysteine / TPAH, calcined	0.178 ± 0.05	1.78	N.D.	N.D.	N.D.
CA-500	Citric acid / NaOH	Not determined	—	—	—	—

N.D. = Not Detected

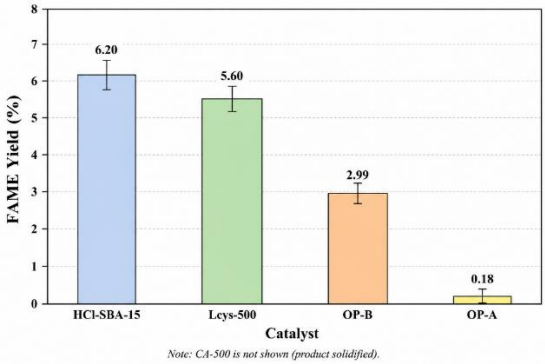

Fig. 6. Bar chart comparing biodiesel yields of different SBA-15 catalysts

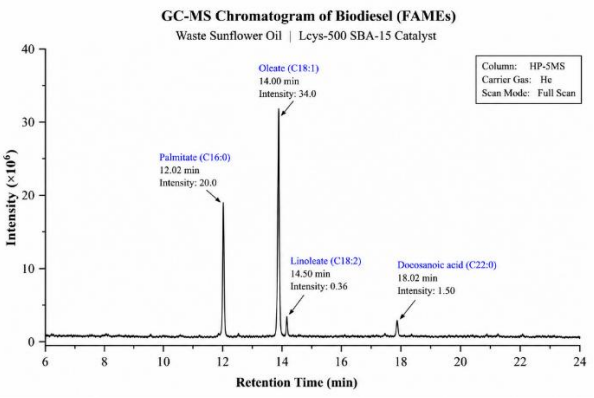

Fig. 7. GC-MS chromatogram of biodiesel from waste sunflower oil using Lcys-500 catalyst

3.9 Green Chemistry Metrics:

The green chemistry metrics comparing the conventional and green SCBA-derived SBA-15 synthesis routes are summarised in Table 7. The use of agricultural waste ash as a silica precursor represents a strong advantage over synthetic TEOS, which is petrochemical-derived and has a significant manufacturing footprint. The substitution of HCl with citric acid or L-cysteine reduces the hazard associated with mineral acid use and lowers the downstream disposal burden. The use of TPAH in the one-pot route combines pretreatment and digestion, avoiding a separate NaOH digestion step[53-55].

However, the green routes show trade-offs. The residual organic content (TGA) is variable: CA-500 shows the lowest residual organics (2–3%), even lower than HCl-SBA-15 (3–4%), while Lcys-500 shows significantly higher residual organics (7–8%). This indicates that citric acid pretreatment effectively removes organic residues, while L-cysteine pretreatment leaves substantial organic matter that is not completely removed during calcination.

The waste streams closed by the green routes are a key advantage. The SCBA-derived materials

address agricultural waste diversion, and the downstream applications (dye adsorption, biodiesel catalysis) close additional waste loops. This represents a genuine circular economy pathway, though the reagent and energy costs must be carefully evaluated.

Table 7. Green chemistry metrics: conventional versus green SCBA-derived SBA-15 synthesis routes

Green-chemistry criterion	HCl-SBA-15 (Conventional)	CA-500 (Green)	Lcys-500 (Green)	OP-A (Green)
Silica precursor	Agricultural waste ash	Agricultural waste ash	Agricultural waste ash	Agricultural waste ash
Pretreatment acid	HCl (mineral acid)	Citric acid (organic acid)	L-cysteine (amino acid)	L-cysteine (amino acid)
Alkaline agent	NaOH (caustic)	NaOH (caustic)	NaOH (caustic)	TPAH (one-pot route)
Residual carbon (EDS, wt%)	9.41	6.73	48.83	24.28
TGA weight loss (%)	~3–4	~2–3	~7–8	~3
Hazardous waste generation	Moderate	Low	Low	Low
Reagent recovery	Not demonstrated	Not demonstrated	Not demonstrated	Not demonstrated
Waste stream(s) closed	Bagasse ash	Bagasse ash	Bagasse ash	Bagasse ash

3.10 Qualitative Circularity Assessment:

A qualitative circularity assessment of the SCBA-to-SBA-15 conversion route is presented in Table 8. The route scores strongly on waste prevention (diverts SCBA from landfills) and renewable feedstock use (ash is a byproduct of existing agricultural processing). However, it scores weak-to-moderate on auxiliary substance use (acid wash and alkaline extraction consume significant NaOH/HCl or citric acid/TPAH volumes with no recovery step reported) and energy use (combustion, extraction reflux, and 24–62 h hydrothermal ageing are each energy-intensive).

The most significant gap is the absence of template (P123) recovery. All five synthesis routes remove the template by calcination (destructive), rather than solvent extraction (recoverable). From a circularity standpoint, calcination is the least resource-efficient template-removal option, since it destroys the surfactant rather than recovering it. Solvent extraction (typically acidified ethanol reflux) would in principle allow P123 recovery and reuse, significantly improving the circularity of the process.

The downstream loop closure is demonstrated directly: dye removal and waste-oil valorisation both close a second waste loop. However, life-cycle and techno-economic data are absent from our study and from the primary studies reviewed. No formal costing or LCA comparison against TEOS-derived material has been reported, representing the most consequential remaining gap for establishing the circular economy case on quantitative grounds[56-58].

Table 8. Qualitative circularity/techno-economic assessment

Circularity dimension	HCl-SBA-15	CA-500	Lcys-500	OP-A
Waste prevention	Strong	Strong	Strong	Strong
Renewable feedstock use	Strong	Strong	Strong	Strong

Auxiliary substance use	Weak	Moderate	Moderate	Moderate
Energy use	Weak	Weak	Weak	Weak
Template (P123) recovery	Not demonstrated	Not demonstrated	Not demonstrated	Not demonstrated
Downstream loop closure (dye adsorption)	Strong	Moderate	Low	Low
Downstream loop closure (biodiesel)	Strong	Not determined	Moderate	Weak
Life-cycle / techno-economic data	Absent	Absent	Absent	Absent
Overall circularity score	**Medium**	**Medium-High**	**Medium**	**Low-Medium**

4. Conclusions

Framing the SCBA-to-SBA-15 conversion as a circular-economy process rather than a simple silica-source substitution clarifies what the route in this literature actually achieves and what it does not achieve.

Achievements:

1. **Successful Synthesis:** Five independent synthesis routes (conventional HCl/NaOH, green CA/NaOH, green L-cys/NaOH, and green TPAH one-pot with and without calcination) confirm that agricultural ash can be converted into structurally recognisable mesoporous silica (BET surface areas of 18–466 m^2/g).
2. **Conventional Route Performance:** The HCl-SBA-15 route produces material with the highest surface area (466 ± 12 m^2/g) and cleanest pore structure (3.12 ± 0.15 nm pores), comparable to TEOS-derived SBA-15 and consistent with the values reported by Norsuraya et al. (2016).
3. **Green Route Advantages:** The green routes using citric acid (CA-500) and L-cysteine (Lcys-500) produce materials with larger pores (14.9–15.6 nm), which may be beneficial for applications requiring diffusion of larger molecules such as bulky dye molecules or oil triglycerides. This represents a tunable property that can be exploited for specific applications.
4. **Environmental Remediation:** The HCl-SBA-15 demonstrates excellent adsorption capacity for brilliant green dye (55.1% removal, 5.51 mg/g uptake), confirming the effectiveness of SCBA-derived SBA-15 for water treatment applications.
5. **Waste Valorisation:** Lcys-500 shows promising catalytic activity in biodiesel production from waste sunflower oil (5.60% FAME yield), demonstrating the feasibility of closing a second waste loop (spent cooking oil) using a catalyst derived from a first waste stream (bagasse ash).

Unresolved Issues and Gaps:

1. **Template Recovery:** Template (P123) recovery is not demonstrated in any of the five synthesis routes. All studies remove the template by calcination (destructive), rather than solvent extraction (recoverable). This represents the single most significant opportunity for improving the circularity of the process.
2. **Green Route Trade-offs:** The 'greener' pretreatment chemistry (L-cysteine, TPAH) does not uniformly reduce residual organic content relative to the conventional HCl/NaOH route. Lcys-500 shows 7–8% residual organics (TGA) compared to 3–4% for HCl-SBA-15, and EDS carbon content of 48.83 wt% compared to 9.41 wt% for HCl-SBA-15. This represents a significant trade-off

between environmental benefits and material quality.

3. **Surface Area Reduction:** The green routes generally produce lower surface areas than the conventional route (95.97–220.37 m^2/g vs. 466 m^2/g). This limits their performance in adsorption applications where high surface area is critical.
4. **Catalyst Performance:** While Lcys-500 shows the best catalytic performance among the green routes (5.60% FAME yield), this is significantly lower than commercial catalysts or functionalized SBA-15. Surface functionalization or metal doping would be required to achieve commercially viable yields.
5. **Life-Cycle Data:** No formal energy or reagent balance is reported in this study or in the primary literature reviewed. A formal life-cycle costing analysis is absent from the published record. This is the most consequential gap for establishing the circular economy case on quantitative grounds.

Future Recommendations:

1. **Solvent-Based Template Recovery:** Future work should explore solvent extraction methods (e.g., acidified ethanol reflux) for P123 recovery and reuse, which would significantly improve the circularity of the process by preserving the surfactant template rather than destroying it through calcination.
2. **Optimisation of Green Routes:** The calcination conditions for L-cysteine and TPAH-derived samples should be optimised (higher temperature, longer time, or oxidising atmosphere) to reduce residual carbon without compromising the mesostructure.
3. **Surface Functionalization:** The catalytic performance of SCBA-derived SBA-15 can be dramatically improved through surface functionalization with sulfonic acid groups or metal doping (Zuo et al., 2013; Chen et al., 2011), which would increase the acid site density and enhance transesterification activity.
4. **Techno-Economic Analysis:** A comprehensive techno-economic analysis and life-cycle assessment comparing SCBA-derived SBA-15 with TEOS-derived material is urgently needed to establish the circular economy case on quantitative grounds.
5. **Standardisation:** Standardised protocols for ash pretreatment across different mills and geographic locations are needed to ensure reproducible material quality and enable industrial scale-up.

The chemistry underlying SCBA-to-SBA-15 conversion is well established and closely tracks the more mature rice-husk-ash literature. What remains is standardising ash pretreatment across mills, closing the template and reagent loops more tightly, and producing the life-cycle data that would let the circular-economy case be argued on quantitative rather than qualitative grounds.

References

1. Abdulazeez, I., Alrajjal, A. S., Ganiyu, S., Baig, N., Salhi, B., &AbdElazem, S. (2023). Facile engineering of mesoporous silica for the effective removal of anionic dyes from wastewater: Insights from DFT and experimental studies. *Heliyon*, 9(11), Article e21356.
2. Alosaimi, E. H., Alsohaimi, I. H., Dahan, T. E., Chen, Q., Younes, A. A., El-Gammal, B., &Melhi, S. (2021). Photocatalytic degradation of methylene blue and antibacterial activity of mesoporous TiO_2-SBA-15 nanocomposite based on rice husk. *Adsorption Science & Technology*, 2021, Article 9290644.
3. Amaraweera, S. M., Gunathilake, C. A., Gunawardene, O. H. P., Dassanayake, R. S., Cho, E.-B., & Du, Y. (2023). Carbon capture using porous silica materials. *Nanomaterials*, 13(14), Article 2050.
4. Anastas, P. T., & Warner, J. C. (1998). *Green chemistry: Theory and practice*. Oxford University Press.
5. Beck, J. S., Vartuli, J. C., Roth, W. J., Leonowicz, M. E., Kresge, C. T., Schmitt, K. D., Chu, C. T.-W., Olson, D. H., Sheppard, E. W., McCullen, S. B., Higgins, J. B., & Schlenker, J. L. (1992). A new family of mesoporous molecular sieves prepared with

liquid crystal templates. *Journal of the American Chemical Society*, 114(27), 10834–10843.

6. Bhagiyalakshmi, M., Yun, L. J., Anuradha, R., & Jang, H. T. (2010a). Synthesis of chloropropylamine-grafted mesoporous MCM-41, MCM-48 and SBA-15 from rice husk ash: Their application to CO_2 chemisorption. *Journal of Porous Materials*, 17(4), 475–484.
7. Bhagiyalakshmi, M., Yun, L. J., Anuradha, R., & Jang, H. T. (2010b). Utilisation of rice husk ash as silica source for the synthesis of mesoporous silicas and their application to CO_2 adsorption through TREN/TEPA grafting. *Journal of Hazardous Materials*, 175(1–3), 928–938.
8. Chen, C., Yang, S. T., Ahn, W. S., & Ryoo, R. (2009). Amine-impregnated silica monolith with a hierarchical pore structure: Enhancement of CO_2 capture capacity. *Chemical Communications*, 2009(24), 3627–3629.
9. Chen, S.-Y., Yokoi, T., Tang, C.-Y., Jang, L.-Y., Tatsumi, T., Chan, J. C. C., & Cheng, S. (2011). Sulfonic acid-functionalized platelet SBA-15 materials as efficient catalysts for biodiesel synthesis. *Green Chemistry*, 13(10), 2920–2930.
10. Chuin, L. X., Kamaruzaman, S., Praveena, S. M., & Yahaya, N. (2024). Recent applications of β-cyclodextrin in selective adsorption of pesticides, heavy metals, and organic pollutants from water samples: Mini review. *Microchemical Journal*, 206, Article 111583.
11. Corma, A. (1997). From microporous to mesoporous molecular sieve materials and their use in catalysis. *Chemical Reviews*, 97(6), 2373–2420.
12. Cui, J., Liang, Y., Yang, D., & Liu, Y. (2016). Facile fabrication of rice husk-based silicon dioxide nanospheres loaded with silver nanoparticles as a rice antibacterial agent. *Scientific Reports*, 6, Article 21423.
13. Cussa, J., Juárez, J. M., Gómez Costa, M. B., &Anunziata, O. A. (2023). LP-SBA-15/ketorolac nanocomposite: Development, characterisation, and mathematical modelling of controlled keto release. *Biointerface Research in Applied Chemistry*, 13, Article 243.
14. Dhaneswara, D., Tsania, A., Fatriansyah, J. F., Federico, A., Ulfiati, R., Muslih, R., &Mastuli, M. S. (2024). Synthesis of mesoporous silica from sugarcane bagasse as adsorbent for colourants using cationic and non-ionic surfactants. *International Journal of Technology*, 15(2), 373–382.
15. Dong, X., Wang, Y., Dan, H., Hong, Z., Song, K., Xian, Q., & Ding, Y. (2017). A facile route to synthesise mesoporous SBA-15 silica spheres from powder quartz. *Materials Letters*, 204, 97–100.
16. Fan, Y., & Jia, X. (2022). Progress in amine-functionalized silica for CO_2 capture: Important roles of support and amine structure. *Energy & Fuels*, 36(3), 1252–1270.
17. Gebretatios, A. G., Banat, F., Witoon, T., & Cheng, C. K. (2024). Synthesis of sustainable rice husk ash-derived nickel-decorated MCM-41 and SBA-15 mesoporous silica materials for hydrogen storage. *International Journal of Hydrogen Energy*, 51, 255–266.
18. He, Y., Guo, X., Qiao, L., et al. (2024). A Rh/SBA-15 catalyst achieved remarkable performance for hydroformylation of formaldehyde. *Brazilian Journal of Chemical Engineering*, 41, 299–308.
19. Henao, W., Jaramillo, L. Y., López, D., Romero-Sáez, M., & Buitrago-Sierra, R. (2020). Insights into the CO_2 capture over amine-functionalized mesoporous silica adsorbents derived from rice husk ash. *Journal of Environmental Chemical Engineering*, 8(5), Article 104362.
20. Huang, G., Mao, D., Zhang, Y., Chen, X. D., & Wu, Z. (2023). Postsynthesis of β-FeOOH/SBA-15 composites via mild ozone treatment: Effective surfactant removal and perfect property preservation for enhanced arsenic adsorption. *Journal of Environmental Chemical Engineering*, 11(2), Article 109597.
21. Huang, Y., Jia, Y., Hou, R., Huang, Z., Shen, K., Jin, G., & Hou, L. (2021). Photocatalytic degradation of unsymmetrical dimethylhydrazine on TiO_2/SBA-15 under 185/254 nm vacuum-ultraviolet. *RSC Advances*, 11(39), 24172–24182.
22. Juárez, J. M., Gómez Costa, M. B., &Anunziata, O. A. (2015). Synthesis and characterisation of Pt-CMK-3 hybrid nanocomposite for hydrogen storage. *International Journal of Energy Research*, 39(1), 128–139.
23. Krajnović, T., Maksimović-Ivanić, D., Mijatović, S., Drača, D., Wolf, K., Edeler, D., Wessjohann, L. A., & Kaluđerović, G. N. (2018). Drug delivery system for emodin based

on mesoporous silica SBA-15. *Nanomaterials*, 8(5), Article 322.

24. Kresge, C. T., Leonowicz, M. E., Roth, W. J., Vartuli, J. C., & Beck, J. S. (1992). Ordered mesoporous molecular sieves synthesised by a liquid-crystal template mechanism. *Nature*, 359(6397), 710–712.
25. Laad, M., Datkhile, R., & Shanmugan, S. (2021). Synthesis and characterisation of powder silica: A judicious recycling of the natural ceramic rice husk ash. *Silicon*. Advance online publication.
26. Lam, H. (2020). Synthesis and characterisation of mesoporous silica SBA-15 and ZnO/SBA-15 photocatalytic materials from the ash of brickyards. *Journal of Chemistry*, 2020, Article 8456194.
27. Léon, C. I. S., Song, D., Su, F., An, S., Liu, H., Gao, J., Guo, Y., & Leng, J. (2015). Propylsulfonic acid and methyl bifunctionalized TiSBA-15 silica as an efficient heterogeneous acid catalyst for esterification and transesterification. *Microporous and Mesoporous Materials*, 204, 218–225.
28. Lewandowski, D., Machnicka, A., et al. (2015). SBA-15 mesoporous silica modified with gallic acid and evaluation of its cytotoxic activity. *PLOS ONE*, 10(7), Article e0132541.
29. Li, D., Chai, K., Yao, X., Zhou, L., Wu, K., Huang, Z., Yan, J., Qin, X., Wei, W., & Ji, H. (2021). β-Cyclodextrin functionalized SBA-15 via amide linkage as a super adsorbent for rapid removal of methyl blue. *Journal of Colloid and Interface Science*, 583, 100–112.
30. Li, D., Min, H., Jiang, X., Ran, X., Zou, L., & Fan, J. (2013). One-pot synthesis of aluminium-containing ordered mesoporous silica MCM-41 using coal fly ash for phosphate adsorption. *Journal of Colloid and Interface Science*, 404, 42–48.
31. Liang, B., Zhu, P., Gu, J., Yuan, W., Xiao, B., Hu, H., & Rao, M. (2024). Advancing adsorption and separation with modified SBA-15: A comprehensive review and future perspectives. *Molecules*, 29(15), Article 3543.
32. Liu, H., Lao, Y., Wang, J., Jiang, J., Yu, C., & Liu, Y. (2022). Rational design of mesoporous silica (SBA-15)/PF (phenolic resin) nanocomposites by tuning the pore sizes of mesoporous silica. *Materials*, 15(24), Article 8879.
33. Melero, J. A., Bautista, L. F., Morales, G., Iglesias, J., & Sánchez-Vázquez, R. (2015). Acid-catalysed production of biodiesel over arenesulfonic SBA-15: Insights into the role of water in the reaction network. *Renewable Energy*, 75, 425–432.
34. Moayedi, H., Aghel, B., Abdullahi, M. M., Nguyen, H., &Safuan, A. R. A. (2019). Applications of rice husk ash as green and sustainable biomass. *Journal of Cleaner Production*, 237, Article 117851.
35. Norsuraya, S., Fazlena, H., &Norhasyimi, R. (2016). Sugarcane bagasse as a renewable source of silica to synthesise Santa Barbara Amorphous-15 (SBA-15). *Procedia Engineering*, 148, 839–846.
36. Rodrigues, J. J., Fernandes, F. A. N., & Rodrigues, M. G. F. (2018). Co/Ru/SBA-15 catalysts synthesised with rice husk ashes as silica source applied in the Fischer–Tropsch synthesis. *Brazilian Journal of Petroleum and Gas*, 12(4), 169–179.
37. Shah, K. A., Parikh, J. K., &Maheria, K. C. (2014). Biodiesel synthesis from acid oil over large pore sulfonic acid-modified mesostructured SBA-15: Process optimisation and reaction kinetics. *Catalysis Today*, 237, 29–37.
38. Shakeri, M., Shal, Z. K., & Van Der Voort, P. (2021). An overview of the challenges and progress of synthesis, characterisation, and applications of plugged SBA-15 materials for heterogeneous catalysis. *Materials*, 14(17), Article 5082.
39. Slowing, I. I., Trewyn, B. G., Giri, S., & Lin, V. S.-Y. (2007). Mesoporous silica nanoparticles for drug delivery and biosensing applications. *Advanced Functional Materials*, 17(8), 1225–1236.
40. Su, G., Xu, Z., et al. (2022). Preparation of mesoporous silica-based nanocomposites with synergistically antibacterial performance from nano-metal (oxide) and polydopamine. *Nanotechnology*, 33(15), Article 155702.
41. Sukirna, I., Dhaneswara, D., Siregar, D. J., Fatriansyah, J. F., Sofyan, N., Yuwono, A. H., & Muslih, R. (2024). Synthesis of mesoporous silica from sugarcane bagasse ash using Pluronic 123 as a colourant adsorbent for brilliant green. *EVERGREEN Joint Journal of Novel Carbon Resource Sciences & Green Asia Strategy*, 11(2), 1366–1374.
42. Taguchi, A., &Schüth, F. (2005). Ordered mesoporous materials in catalysis. *Microporous and Mesoporous Materials*, 77(1), 1–45.

43. Thenaruvi, D., Jeya Sundara Sharmila, D., Shanmugapriya, S., & Lakshmanan, A. (2021). Synthesis and characterisation of mesoporous silica from sugarcane bagasse industrial fly ash. *International Journal of Ecology and Environmental Sciences*, 3(1), 81–86.

44. Vallet-Regí, M., Colilla, M., Izquierdo-Barba, I., & Manzano, M. (2018). Mesoporous silica nanoparticles for drug delivery: Current insights. *Molecules*, 23(1), Article 47.

45. Vinu, A., Mori, T., & Ariga, K. (2006). New families of mesoporous materials. *Science and Technology of Advanced Materials*, 7(8), 753–771.

46. Wang, L., He, H., Zhang, C., Sun, L., Liu, S., & Yue, R. (2014). Excellent antimicrobial properties of silver-loaded mesoporous silica SBA-15. *Journal of Applied Microbiology*, 116(5), 1106–1118.

47. Wang, S., Zheng, Y., & Lang, M. (2024). Preparation of hydrotalcite/SBA-15 composite catalyst and its application in the synthesis of ε-caprolactone. *Catalysis Letters*, 154, 6094–6105.

48. Xu, Q., Ji, T., Gao, S. J., Yang, Z., & Wu, N. (2018). Characteristics and applications of sugar cane bagasse ash waste in cementitious materials. *Materials*, 12(1), Article 39.

49. Yang, L., Wang, B., Lai, S., Jiang, C., & Zhong, H. (2015). Enhancing photocatalytic degradation of phenol through nitrogen- and nitrogen/fluorine-codoped Ti-SBA-15. *RSC Advances*, 5(66), 53299–53305.

50. Yu, X., Li, H., Yu, T., Weng, Q., Zhao, Z., & Xia, Z. (2022). Preparation and application of metal oxides/SBA-15 mesoporous composites as catalysts for selective oxidation of benzyl alcohol. *International Journal of Electrochemical Science*, 17(1), Article 220114.

51. Yuan, S., Wang, M., Liu, J., & Guo, B. (2020). Recent advances of SBA-15-based composites as the heterogeneous catalysts in water decontamination: A mini-review. *Journal of Environmental Management*, 254, Article 109787.

52. Zhao, D., Feng, J., Huo, Q., Melosh, N., Fredrickson, G. H., Chmelka, B. F., & Stucky, G. D. (1998). Triblock copolymer syntheses of mesoporous silica with periodic 50 to 300 angstrom pores. *Science*, 279(5350), 548–552.

53. Zhao, D., Huo, Q., Feng, J., Chmelka, B. F., & Stucky, G. D. (1998). Nonionic triblock and star diblock copolymer and oligomeric surfactant syntheses of highly ordered, hydrothermally stable, mesoporous silica structures. *Journal of the American Chemical Society*, 120(24), 6024–6036.

54. Zhu, X., Xie, W., Wu, J., Miao, Y., Xiang, C., Chen, C., Ge, B., Gan, Z., Yang, F., Zhang, M., O'Hare, D., Li, J., Ge, T., & Wang, R. (2022). Recent advances in direct air capture by adsorption. *Chemical Society Reviews*, 51(15), 6574–6651.

55. Zuo, D., Lane, J., Culy, D., Schultz, M., Pullar, A., & Waxman, M. (2013). Sulfonic acid functionalized mesoporous SBA-15 catalysts for biodiesel production. *Applied Catalysis B: Environmental*, 129, 342–350.